PNAS RESEARCH ARTICLE | APPLIED BIOLOGICAL SCIENCES CHEMISTRY

Targeted glycan degradation potentiates cellular immunotherapy for solid tumors

Jicheng Wu[a,b,c,1], Xudong Wang[d,e,1], Yuqiao Huang[a,b,1], Yunjing Zhang[f], Siyu Su[e,g], Hao Shou[a,b], Haoran Wang[a,b], Jin Zhang[d,e,2], and Ben Wang[a,b,h,2]

Edited by Carl June, University of Pennsylvania, Philadelphia, PA; received January 8, 2023; accepted August 8, 2023

Immune cell–based cancer therapies, such as chimeric antigen receptor T (CAR-T)-cell immunotherapy, have demonstrated impressive potency against hematological tumors. However, the efficacy of CAR-T cells against solid tumors remains limited. Herein, we designed tumor-targeting molecule–sialidase conjugates that potently and selectively stripped different sialoglycans from a variety of cancer cells. Desialylation enhanced induced pluripotent stem cell–derived chimeric antigen receptor–macrophage (CAR-iMac) infiltration and activation. Furthermore, the combination of cancer cell desialylation and CAR-iMac adoptive cellular therapy exerted a dramatic therapeutic effect on solid tumors and significantly prolonged the survival of tumor-bearing mice; these effects were mainly dependent on blockade of the checkpoint composed of sialic acid–binding immunoglobulin-like lectin (Siglec)-5 and Siglec-10 on the macrophages, and knockout of the glycoimmune checkpoint receptors could construct a CAR-iMac cell with stronger anticancer activity. This strategy that reverts the immune escape state ("cold tumor") to a sensitive recognition state ("hot tumor") has great significance for enhancing the effect of cellular immunotherapy on solid tumors. Therefore, desialylation combined with CAR-iMac cellular immunotherapy is a promising approach to enhance treatment with cellular immunotherapy and expand the valid indications among solid tumors, which provides inspiration for the development of cellular immunotherapies with glycoimmune checkpoint inhibition for the treatment of human cancer.

cellular immunotherapy | desialylation | sialic acid | Siglecs | solid tumors

Sialic acid is a negatively charged 9-carbon sugar that is commonly expressed on the cell membranes of all eukaryotic organisms (1). The prominent location of sialic acid on the cell membrane allows it to efficiently participate in cell–extracellular matrix interactions, including adhesion, migration, and immune responses (2). The position of sialic acid on the surface of cells (or some glycoproteins and mucins) determines that it plays the role of stabilizing molecules and molecular membranes and is also an important media tool for communication between cells and the external environment ("antenna molecules"). First, sialic acid can protect molecules or cells from attack by proteases and glycosidases, prolonging their life cycle and function (3). Another possible important function is its antirecognition ability. By forming glycosidic bonds with the ends of cell surface sugar complexes, sialic acid can effectively mask antigens and recognition sites on the cell surface, preventing cells from being recognized and phagocytized by the immune system (4). Young cells in the human body tend to have more sialic acid residues than aging cells (5). Previous studies showed that erythrocytes treated with sialidase had a survival time of only 72 h in reinfused mice, while untreated mouse erythrocytes could last for 40 d (6).

In the process of tumor evolution, tumor cells of different origins express sialic acid to different degrees on membrane glycoproteins and glycolipids and can secrete sialic acid into the tumor microenvironment (TME), which is one of the factors involved in the complexity of the TME. Numerous studies have shown that sialic acid on the surface of cancer cells is highly expressed, and tumor cells with high expression of sialic acid have certain advantages in the malignant growth of cells and are positively correlated with poor prognosis of patients (7). Abnormally high expression of sialic acid confers advantages on tumor cells ranging from inhibition of apoptosis to chemoresistance to cancer therapy. In addition, there are specialized receptor families on the cell membrane that can recognize sialopolysaccharides, such as selectins or sialic acid–binding immunoglobulin-like lectins (Siglecs). Selectins are expressed on endothelial cells, leukocytes, and immune cells and extravasate to sites of inflammation, contributing to the hemogenic spread of cancer cells. Siglecs are expressed in most cells of the immune system and can transmit immune inhibition signals after binding to sialic acid ligands (8). The increase in tumor cell affinity to the Siglec may be one of the mechanisms of tumor cell immune escape. Discovering new immune checkpoint molecules that regulate the functions of adaptive and innate immune cells in various tumors, clarifying the

Significance

The upregulation of sialoglycans is a phenomenon that contributes to the long circulation of red cells and convenient migration of stem and cancer cells. Inspired by this, we designed tumor-targeting molecule–sialidase conjugates that selectively stripped different sialoglycans from a variety of cancer cells. Desialylation of cancer cells triggered CAR-iMac cell activation, increased donor cell polyfunctionality, and enhanced antitumor efficacy against solid tumors, which depends on the blockade of the Siglec-5 and Siglec-10 checkpoints on CAR-iMac cells. Siglec-5 and Siglec-10 gene knockouts allowed for the construction of a CAR-iMac with stronger anticancer activity due to glycoimmune checkpoint blocking. The cancer cell desialylation strategy that reverts the immune escape state is significant for enhancing the effect of solid tumor cellular immunotherapy.

Author contributions: B.W. designed research; J.W., X.W., Y.H., Y.Z., S.S., H.S., and H.W. performed research; J.W., X.W., H.S., J.Z., and B.W. contributed new reagents/analytic tools; J.W., X.W., Y.H., Y.Z., S.S., H.W., and B.W. analyzed data; and J.W., J.Z., and B.W. wrote the paper.

Competing interest statement: The subject matter described in this article is included in a patent application filed by Zhejiang University. J.Z. is a scientific cofounder of CellOrigin. None of the conflicts affected the experimental design, interpretation, and reporting of the results. The other authors declare no competing interest.

This article is a PNAS Direct Submission.

[1]J.W., X.W., and Y.H. contributed equally to this work.

[2]To whom correspondence may be addressed. Email: benwang@zju.edu.cn or zhgene@zju.edu.cn.

This article contains supporting information online at https://www.pnas.org/lookup/suppl/doi:10.1073/pnas.2300366120/-/DCSupplemental.

Published September 11, 2023.

regulatory mechanism of their function, and exploring the similarities, differences, and interconnections (synergy, complementarity, compensation, etc.) between the new molecules and known immune checkpoint molecules such as programmed death-ligand 1 (PD-L1), cytotoxic T lymphocyte-associated antigen-4 (CTLA-4), and CD47 are urgently needed.

Here, we demonstrated the inhibitory roles of the cell-surface glycocalyx in antibody-dependent cellular phagocytosis (ADCP) and cell-mediated cytotoxicity (ADCC), and targeted removal of these cell-surface polysaccharides significantly enhanced tumor cell susceptibility. Bone marrow– or peripheral blood mononuclear cell (PBMC)–derived primary macrophages are not efficiently engineered, thus leaving induced pluripotent stem cell (iPSC)–derived macrophages as a great source for myeloid cell–based immunotherapy (9, 10). Furthermore, tumor-targeting molecule–sialidase conjugates can potently and selectively strip different sialoglycans from a variety of cancer cells, and desialylation enhanced the infiltration and activation of iPSC-derived CAR-macrophages (CAR-iMacs), resulting in potent cancer cell killing and significantly prolonged survival in ovarian cancer mouse models. These effects were mainly dependent on checkpoint blockade targeting highly expressed Siglecs, including Siglec-5 and Siglec-10, as their genetic depletion led to enhanced anticancer activity. Therefore, glycoimmune checkpoint inhibition, such as desialylation combined with CAR-based cellular immunotherapy, is a promising approach to achieving the killing efficiency of cellular immunotherapy against solid tumors.

Results

Roles of the Cell-Surface Glycocalyx in ADCP and ADCC. The surface of cancer cells is abnormally hypersialylated, and upregulation of sialic acids is correlated with the growth, adhesion, metastasis, and decreased immunogenicity of tumors. In cancer cells, overexpression of sialyltransferases (ST6GAL1, ST3GAL1, and ST3GAL6) or glycosylase (glucosamine (UDP-N-acetyl)-2-epimerase/N-acetylmannosamine kinase, GNE) leads to increased synthesis of sialoglycoconjugates that are deposited on the cell surface (11–13). It is possible that overexpression of sialyltransferases also leads to the neoformation of cancer sialoglycans. Analysis of mRNA expression data from the Oncomine and The Cancer Genome Atlas (TCGA) databases showed that the *ST6GAL1*, *ST3GAL1*, *ST3GAL6,* and *GNE* levels were significantly up-regulated in tumor tissues compared to healthy tissues across many human cancer types (*SI Appendix*, Fig. S1 *A*–*C*). Furthermore, those mRNA levels were consistently up-regulated in some solid tumors, such as ovarian carcinoma, compared to healthy control tissue (*SI Appendix*, Fig. S1*D*). Regrettably, there was no quantitative analysis of sialic acid expression on the surface of cancer cells. Here, we employed a simple and reliable method to assess the sialylation level of a variety of glycans. Dissociative sialic acid was released from glycoproteins by an efficient sialidase and labeled with 1,2-diamino-4,5-methylenedioxybenzene (DMB) in vitro. Then, high-performance liquid chromatography (HPLC) was used to detect the structures of sialic acid (*SI Appendix*, Fig. S2*A*). To confirm that the efficient sialidase could completely remove sialic acid from cell-surface glycans, we tested its effects on fluorescein isothiocyanate (FITC)-*Sambucus nigra* agglutinin (SNA) labeling of pancreatic cancer cells (*SI Appendix*, Fig. S2 *B* and *C*). Desialylation of pancreatic cancer cells by highly active sialidase significantly reduced the binding of SNA (*SI Appendix*, Fig. S2*C*). A DMB-sialic acid reference panel chromatogram displayed all the variation structures of sialic acid (*SI Appendix*, Fig. S2*D*). According to an optimal standard quasi curve (*SI Appendix*, Fig. S2*E*), we calculated the content of sialic acid on the cell surface for multiple cancer cell lines and found that the surface sialic acid content of cancer cells was generally higher than that of adjacent normal cells, and there were differences among the cancer cell lines. Interestingly, highly malignant cancer cells, such as pancreatic cancer cells, seemed to have higher levels of glycosylation (Fig. 1*A*).

To determine the effects of sialidase treatment on cancer cell susceptibility to ADCC, we first assayed the cytoactivity of pancreatic cancer cells after removal of glycosylation by sialidase. The proliferative and apoptotic activities of pancreatic cancer cells were not significantly affected when the high glycosylation on the surface of the cancer cells was completely removed (*SI Appendix*, Fig. S3 *A* and *B*), but deglycosylation did slightly increase the permeability of cancer cells (*SI Appendix*, Fig. S3*C*).

ADCP critically contributes to the efficacy of antitumor therapy and plays a fundamental role in innate immune surveillance for cancerous growth. Ovarian cancer is among the most lethal diseases affecting women, with few targeted therapies and high rates of metastasis, and cancer cells are capable of evading clearance by macrophages through overexpression of antiphagocytic surface proteins called "don't eat me" signals, which include Siglecs (14). To determine the effects of the glycocalyx on cancer cell susceptibility to phagocytosis, we successfully developed iPSC-derived and mesothelin (MSLN)-specific CAR-expressing CAR-iMacs as described previously (*SI Appendix*, Fig. S4) (9). MSLN is a cell-surface antigen that is highly expressed across a wide range of solid tumors, including ovarian cancer (15). MSLN-CAR expression conferred antigen-dependent macrophage functions, such as the expression and secretion of cytokines, polarization toward the proinflammatory/antitumor state, and enhanced phagocytosis of tumor cells. We analyzed mRNA expression data from the Oncomine and TCGA databases and demonstrated that *MSLN* levels were significantly up-regulated across many human cancer types and that among them, ovarian cancer was the most prominent (*SI Appendix*, Fig. S5*A*). In addition, *MSLN* mRNA levels were consistently and significantly up-regulated in ovarian carcinoma tissue compared to healthy controls (*SI Appendix*, Fig. S5 *B* and *C*), and ovarian cancer patients with high mRNA expression of *MSLN* had a worse long-term prognosis (*SI Appendix*, Fig. S5*D*). To further clarify the impact of sialylation on macrophage-mediated cytotoxicity to cancer cells, we cocultured normal CAR-iMacs or M1 polarized CAR-iMacs with the ovarian cancer cell line SKOV3 in vitro after cancer cell deglycosylation with sialidase pretreatment. Remarkably, deglycosylation of cancer cells significantly promoted the CAR-iMac-mediated tumor cytotoxicity, despite the fact that macrophages had been significantly activated by interferon (IFN)-γ and lipopolysaccharide (LPS) (Fig. 1*B*). In addition, deglycosylation of cancer cells also facilitated phagocytosis (Fig. 1*C*) and increased the formation of phagosomes (Fig. 1*D*). Interestingly, cancer cell deglycosylation also prominently increased the polarization of CAR-iMacs in vitro (Fig. 1*E*), consistent with the ability of CAR-iMacs to secrete cytotoxic cytokines such as tumor necrosis factor (TNF)-α, interleukin (IL)-1β, and IFN-γ (Fig. 1*F* and *SI Appendix*, Fig. S5*E*).

Natural killer (NK) cells are innate cytotoxic lymphocytes involved in the surveillance and elimination of cancer. NK-92MI cells are a nonimmunogenic NK-cell line with constitutive cytotoxic activity that are widely used in ADCC assays. To clarify the role of the cell-surface glycocalyx in ADCC, the cytotoxic efficiency of NK-92MI cells against human pancreatic cancer Panc1 cells, which have high glycosylation, was assessed by quantifying the formation of cell–cell conjugates in cocultures. As expected, sialidase treatment significantly potentiated the killing response at various effector/target (E/T) ratios (*SI Appendix*, Fig. S6*A*), with the most pronounced effect observed with BxPC3 cells (Fig. 1*G*). Consistently, deglycosylation of cancer cells significantly stimulated NK-92MI cell expression (*SI Appendix*, Fig. S6*B*) and secretion of

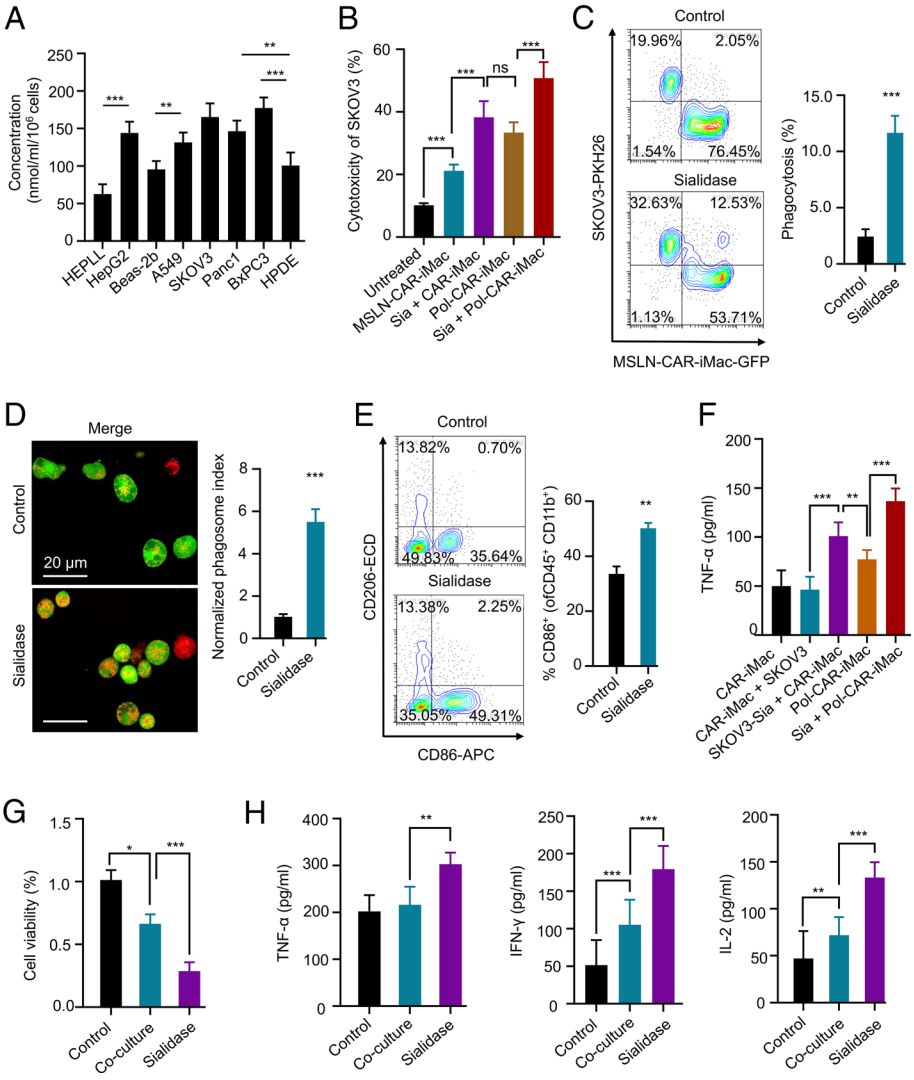

Fig. 1. Roles of cancer cell glycosylation in ADCP and ADCC. (*A*) The content of sialic acid on the surface of multiple cancer cell lines. (*B*) Cytotoxicity of CAR-iMacs or polarized CAR-iMacs to SKOV3 cells in the absence or presence of free sialidase at an E/T ratio of 10:1. (*C*) Phagocytosis of SKOV3 cells by CAR-iMacs in the absence or presence of free sialidase (50 nM) at an E/T ratio of 5:1. (*D*) Phagosomes of CAR-iMacs coincubated with SKOV3 cells. (*E*) The polarization state of CAR-iMacs after coculture with deglycosylated cancer cells. (*F*) The concentration of TNF-α in the supernatant of CAR-iMacs or M1 CAR-iMacs coincubated with SKOV3 cells in the absence or presence of free sialidase. SKOV3-Sia represents SKOV3 cells after treatment with sialidase (50 nM). Pol-CAR-iMacs represent polarized macrophages induced by IFN-γ (50 ng/mL) for 4 h. (*G*) Cytoactivity of pancreatic cancer BxPC3 cells alone or coincubated with NK-92MI cells in the absence or presence of free sialidase (50 nM) at an E/T ratio of 5:1. (*H*) The concentrations of TNF-α, IFN-γ, and IL-2 in the supernatant of NK-92MI cells coincubated with BxPC3 cells in the absence or presence of free sialidase (50 nM) at an E/T ratio of 5:1. All data are expressed as the mean ± SD and were analyzed by one-way ANOVA with multiple comparisons correction (*P < 0.05, **P < 0.01, ***P < 0.001).

cytotoxic cytokines (Fig. 1*H*); mechanistically, the desialylation of pancreatic cancer cell lines by sialidase reduced the binding of the NK-cell inhibitory receptors Siglec-7 and Siglec-9 (*SI Appendix*, Fig. S6*C*) to sialylated glycans while increasing binding to the NK-cell activating receptor NKG2D (*SI Appendix*, Fig. S6*D*). These data indicated that hypersialylated cancer cells might not elicit effective ADCP or ADCC and that this hypersialyation could be reversed by treatment with highly effective sialidase.

Deglycosylation of Cancer Cells Increases NK Cell and M1 Macrophage Infiltration in the TME. For in vivo testing of the effects of sialidase treatment on cancer cell susceptibility and growth, we selected the syngeneic Lewis carcinoma model established with C57BL/6 mice and sought to target sialidase to Lewis cells via non-small cell lung cancer–targeting peptide (TP) (16) conjugation (*SI Appendix*, Fig. S7). ^{1}H-NMR spectroscopy, Raman spectra, and Fourier transform infrared spectroscopy (FTIR) analysis all confirmed that sialidase was covalently linked to non-small cell lung cancer-TP (*SI Appendix*, Fig. S8 *A–C*). Concurrently, we evaluated the sialidase activity of sialidase conjugated to TP (TP-Sia) by assessing fluorogenic SNA on the cell surface in an in vitro assay. Notably, the enzymatic activity of TP-Sia remained after the chemical conjugation process (Fig. 2*A*).

We next evaluated the effects of TP-Sia administration on tumor growth in mice. Lewis cells coexpressing luciferase and green fluorescent protein (LLC-luci-GFP) were systemically injected into mice, followed by intravenous (i.v.) treatment with TP-Sia, TP, sialidase (15 mg kg^{-1} per mouse), or phosphate-buffered saline (PBS) (Fig. 2*B*). A slight but not significant antitumor effect and reduced number of tumor nodules in the lungs were observed with TP-Sia treatment, and mouse survival was also extended marginally (Fig. 2 *C–E*). However, the sialic acid residues exposed on the tumor cell surface showed decreased labeling in the TP-Sia-treated tumors compared to the PBS- or TP-treated tumors after the final conjugate injections (Fig. 2*F* and *SI Appendix*, Fig. S9*A*). These data indicate that TP-Sia efficiently desialylated the TME, but deglycosylation of cancer cells alone did not markedly delay tumor growth in vivo. This might be because the tumor cells could constantly synthesize or modify new glycans, making depletion of sialic acid residues by sialidase temporary. Specifically, in vitro, TP-Sia cleaved sialoglycans from Lewis cells, causing an observable increase in NK cell or M1 macrophage infiltration in the TME (Fig. 2*G* and *SI Appendix*, Fig. S9*B*). Consistent with the flow cytometry results, deglycosylation of cancer cells increased the expression levels of NK cell biomarkers but decreased the expression levels of the M2 marker CD206 within the TME (*SI Appendix*, Fig. S10). These encouraging results inspired us to explore the therapeutic effect of deglycation combined with cellular immunotherapy on refractory tumors in vivo.

Deglycosylation of Cancer Cells Promotes Phagocytosis and Antitumor Effects Mediated by Macrophages In Vivo. Next, we performed in vivo experiments with a peritoneal implantation

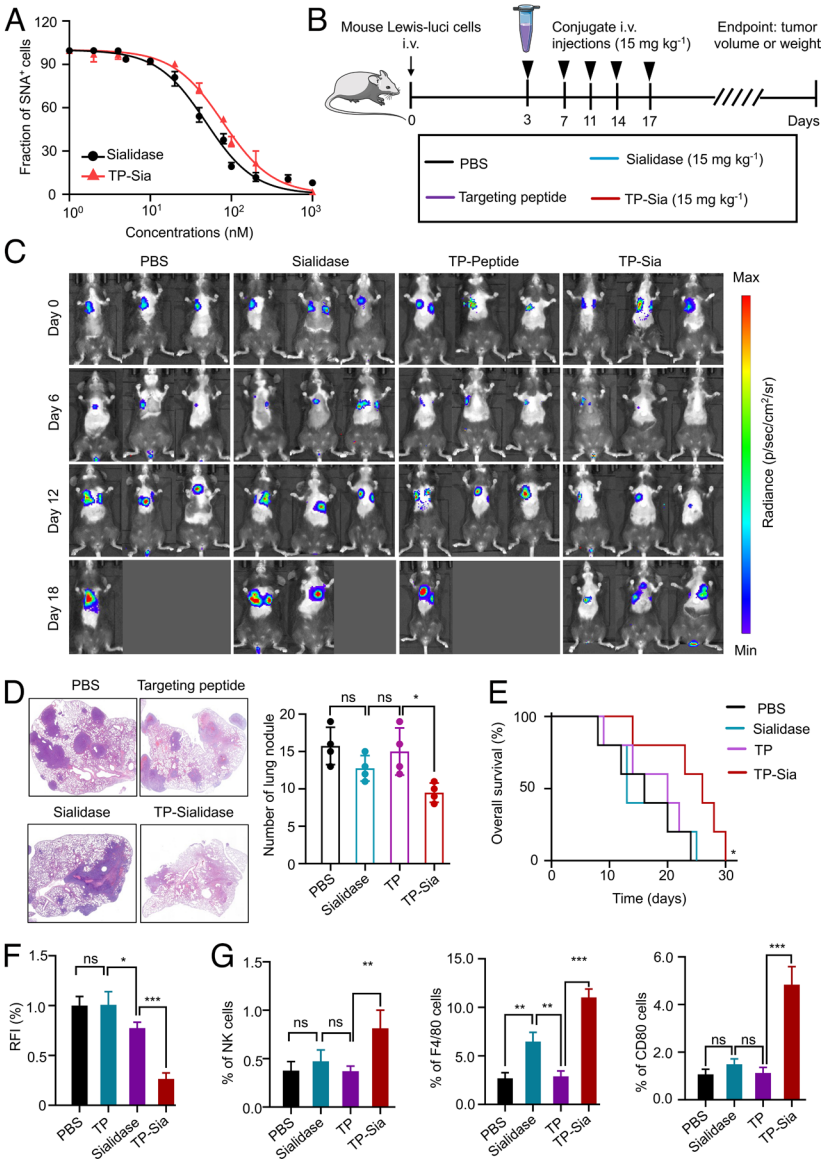

Fig. 2. Deglycosylation of cancer cells increases NK cell and M1 macrophage infiltration in the TME and delays tumor growth in vivo**.** (*A*) Fraction of sialylated (SNA^+) cells quantified by flow cytometry gating after treatment with various concentrations of TP-Sia conjugates. (*B*) Timeline for the intraperitoneal metastasis and cellular immunotherapy mouse model. (*C*) Bioluminescence images of mice subjected to the different treatments. (*D*) Visual quantification of macro- and micrometastases in the lungs of each mouse in all the groups. (*E*) Survival of mice after TP-sialidase conjugate therapy illustrated by Kaplan–Meier curves (**P* < 0.05). (*F*) Fluorescence staining for free sialic acid in tumors. (*G*) Frequencies of immune cells in LLC tumors from PBS-, TP-, sialidase- and TP-Sia-treated mice on day 10. NK cells were defined as $CD45^+CD3^-NKp46^+$, M1 macrophages were defined as $CD45^+CD3^-CD80^+$, and total macrophages were defined as $CD45^+CD3^-F4/80^+$. All data are expressed as the mean ± SD and were analyzed by one-way ANOVA with multiple comparisons correction (**P* < 0.05, ***P* < 0.01, ****P* < 0.001).

model to assess the effect of sialylation on CAR-iMac-mediated cytotoxicity to metastatic ovarian cancer (Fig. 3*A*). An MSLN-CAR plasmid was transfected into iPSCs, and the cells were induced to differentiate into CAR-macrophages in vitro successfully (Fig. 3*B*). Because the peritoneal implantation of ovarian cancer is one of the most common metastases for ovarian cancer and the cancer cells in the abdominal cavity could be directly contacted by sialidase, we removed the glycosylation of SKOV3-luci cells by direct intraperitoneal injection of sialidase without modification before MSLN-CAR-iMac cellular immunotherapy was applied, and tumor growth was monitored by longitudinal, noninvasive bioluminescence imaging (Fig. 3*C*). Compared to the control group that received buffer injection only, the group treated with sialidase only did not show significant inhibition of SKOV3-Luci tumor growth. However, adoptive transfer of MSLN-CAR-iMacs exhibited moderate capacities to suppress tumor growth measured as bioluminescence signals and prolong survival. Notably, deglycosylation of cancer cells combined with adoptive transfer of MSLN-CAR-iMacs displayed surprising efficacy in inhibiting tumor growth (Fig. 3 *C* and *D*) and impressively extended survival time (Fig. 3*E*). Consistent with this knowledge, we collected fluid from the abdominal cavity and analyzed the secretion of cytokines, which demonstrated that deglycosylation of ovarian cancer cells primarily stimulated CAR-iMacs to significantly increase the secretion of cytotoxic cytokines such as TNF-α, IL-1β, and IFN-γ (Fig. 3*F*). These results suggested that deglycosylation of cancer cells might abolish the interaction of sialylated glycans and inhibitory receptors on macrophages, thereby enhancing tumor cell susceptibility to CAR-iMac-mediated phagocytosis.

Deglycosylation Combined with CAR-iMac Cellular Immunotherapy Demonstrated Remarkable Therapeutic Efficacy in Solid Tumors. To accurately mimic the TME of solid tumors and further explore the therapeutic effect of CAR-iMacs combined with deglycosylation on solid tumors, we constructed an orthotopic tumor model of mouse ovarian cancer and modified sialidase for selective targeting following in vivo intravenous injection. Folate receptor (FR) has been reported to exhibit restricted expression in normal tissues but overexpression in multiple solid tumors, especially ovarian tumors, suggesting that folate may be a good ligand for cancer cell targeting. We explored the mRNA expression levels of *FOLR1* in data from the Oncomine and TCGA databases and found that *FOLR1* was significantly up-regulated across many human cancer types and that among them, ovarian cancer was the most prominent (*SI Appendix*, Fig. S11*A*). Furthermore, *FOLR1* mRNA levels were consistently up-regulated in ovarian carcinoma

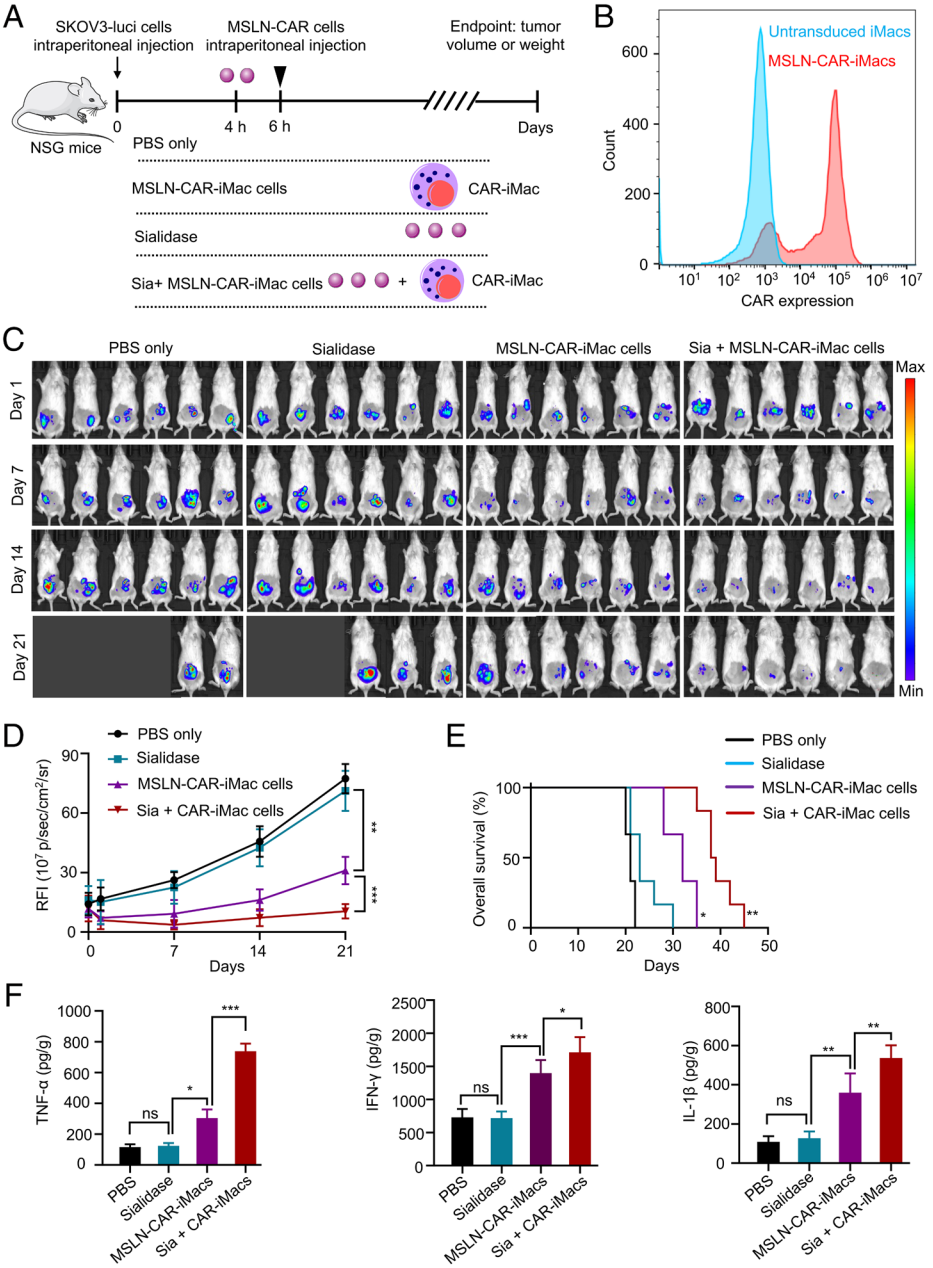

Fig. 3. Deglycosylation of cancer cells promotes phagocytosis and antitumor effects mediated by macrophages in vivo. (*A*) Timeline for the intraperitoneal metastasis and cellular immunotherapy mouse model. (*B*) MSLN-CAR expression on the surface of CAR-iMacs measured by flow cytometry analysis. (*C*) Bioluminescence images of mice subjected to the different treatments. (*D*) Relative fluorescence signal measured by bioluminescence imaging for the different groups. (*E*) Survival of mice after CAR-iMac cellular therapy illustrated by Kaplan–Meier curves. (*F*) The levels of inflammatory factors in mouse peritoneal effusions and tumors from different groups. All data are expressed as the mean ± SD and were analyzed by one-way ANOVA with multiple comparisons correction (*$P < 0.05$, **$P < 0.01$).

tissue compared to healthy control tissue (*SI Appendix*, Fig. S11*B*), and ovarian cancer patients with high mRNA expression of *FOLR1* had a poor long-term prognosis (*SI Appendix*, Fig. S11*C*). In addition, the ovarian cancer cell line SKOV3 we selected for mouse modeling exhibited high expression of both MSLN and FR (*SI Appendix*, Fig. S11*D*), indicating that the adoptive transfer of MSLN-CAR-expressing macrophage cells for cellular therapy and folate-guided deglycosylation were both superiorly selective for ovarian cancer cell lines. We linked the sialidase polymer and folate (FA) to form an FA-Sia molecule complex through a mild reaction and purification system (*SI Appendix*, Fig. S12*A*), and the ^{1}H-NMR spectra of FA-Sia confirmed that the complex was synthesized successfully (*SI Appendix*, Fig. S12*B*). Concurrently, we evaluated the sialidase activity of FA-Sia by an in vitro fluorogenic assay and demonstrated that the enzymatic activity of FA-Sia was mainly retained after the chemical conjugation process (*SI Appendix*, Fig. S12*C*).

Then, using an orthotopic mouse model of ovarian tumors, we assessed the therapeutic potential of targeted deglycosylation of cancer cells in conjunction with adoptive transfer of CAR-iMacs. A small number of SKOV3-luci cells were gently injected into the mouse ovaries in situ to construct solid tumors in the ovary, followed by two i.v. injections of FA-Sia, CAR-iMacs, or FA-Sia combined with CAR-iMacs (*SI Appendix*, Fig. S12*D*). Tumor growth was monitored by longitudinal, noninvasive bioluminescence imaging after the highly active substrate diphenylterazine was injected intraperitoneally. The results demonstrated that a slight but significant antitumor effect was observed after adoptive transfer of CAR-iMacs, and the survival rate of tumor-bearing mice was also marginally extended. Notably, cancer cell deglycosylation combined with adoptive transfer of CAR-iMacs displayed surprisingly strong antitumor efficacy in inhibiting ovarian cancer growth (Fig. 4 *A* and *B*). Consistent with this tumor growth inhibition, FA-Sia-induced desialylation combined with adoptive CAR-iMac cellular therapy significantly prolonged mouse survival (Fig. 4*C*).

To determine whether FA-Sia preferentially accumulates in and destroys sialoglycans on ovarian tumors in mice, we detected the number of sialic acid residues in tumors 48 h after FA-Sia

monotherapy or FA-Sia and CAR-iMac combination treatment (all administered intravenously). We found that the two treatments, including FA-Sia, efficiently degraded tumor sialoglycans (Fig. 4*D*). Remarkably, deglycosylation of cancer cells promoted more macrophage infiltration in the cancer nest (Fig. 4*E* and *SI Appendix*, Fig. S13), and more tumor necrosis–related cytokines such as TNF-α were consistently detected in the combined treatment group (Fig. 4*F*). These results suggested that the surface glycocalyx of cancer cells might contain vital inhibitory ligands (don't eat me signals) that resist phagocytosis or polarization and that targeting clearance of these inhibitory ligands could facilitate "cold tumors" becoming "hot tumors."

Deglycosylation of Cancer Cells Promotes Phagocytosis and Antitumor Effects Mainly via Siglec-5 and Siglec-10 Recognition. To further elucidate the mechanism of how cancer cell deglycosylation enhances the antitumor effects of CAR-iMac, we performed RNA sequencing (RNA-seq) of MSLN-CAR-iMacs on different differentiation days. As summarized in the heatmap (Fig. 5*A*), with the maturation and differentiation of macrophages following induction, MSLN-CAR-iMacs expressed more inhibitory ligand mRNA transcripts, including highly expressed *Siglec-1*, *Siglec-10*, and *Siglec-15*, as well as other *Siglecs*. We further detected the protein levels of the highly expressed Siglecs and surprisingly found that, compared with those in naive cells, the protein expression levels of Siglec-1, Siglec-5, Siglec-10, and Siglec-15 in MSLN-CAR-iMacs presented trends of a significant increase during differentiation and maturation (Fig. 5*B*). Interestingly, the mRNA expression levels of *Siglec-5* and *Siglec-10* were further increased after mature macrophages were cocultured with K562 cancer cells (Fig. 5*C*). Since the CAR-iMac cells were normally used at day 28 in the differentiation process, we hypothesized that these highly expressed Siglecs would typically attenuate macrophage activation and phagocytosis when binding sialic acid. Consistently, using monoclonal antibodies to block Siglec-5 and Siglec-10 on the surface of mature CAR-iMac cells achieved markedly enhanced cytotoxicity similar to cancer cell deglycosylation (Fig. 5*D*). Furthermore, the desialylation of SKOV3 ovarian cancer cells by sialidase treatment significantly reduced the binding of fluorescence-labeled Siglec-5-Fc and Siglec-10-Fc chimeras (Fig. 5*E* and *SI Appendix*, Fig. S14*A*). We then assessed the feasibility of using the Neu5Acα (2–3) Gal of

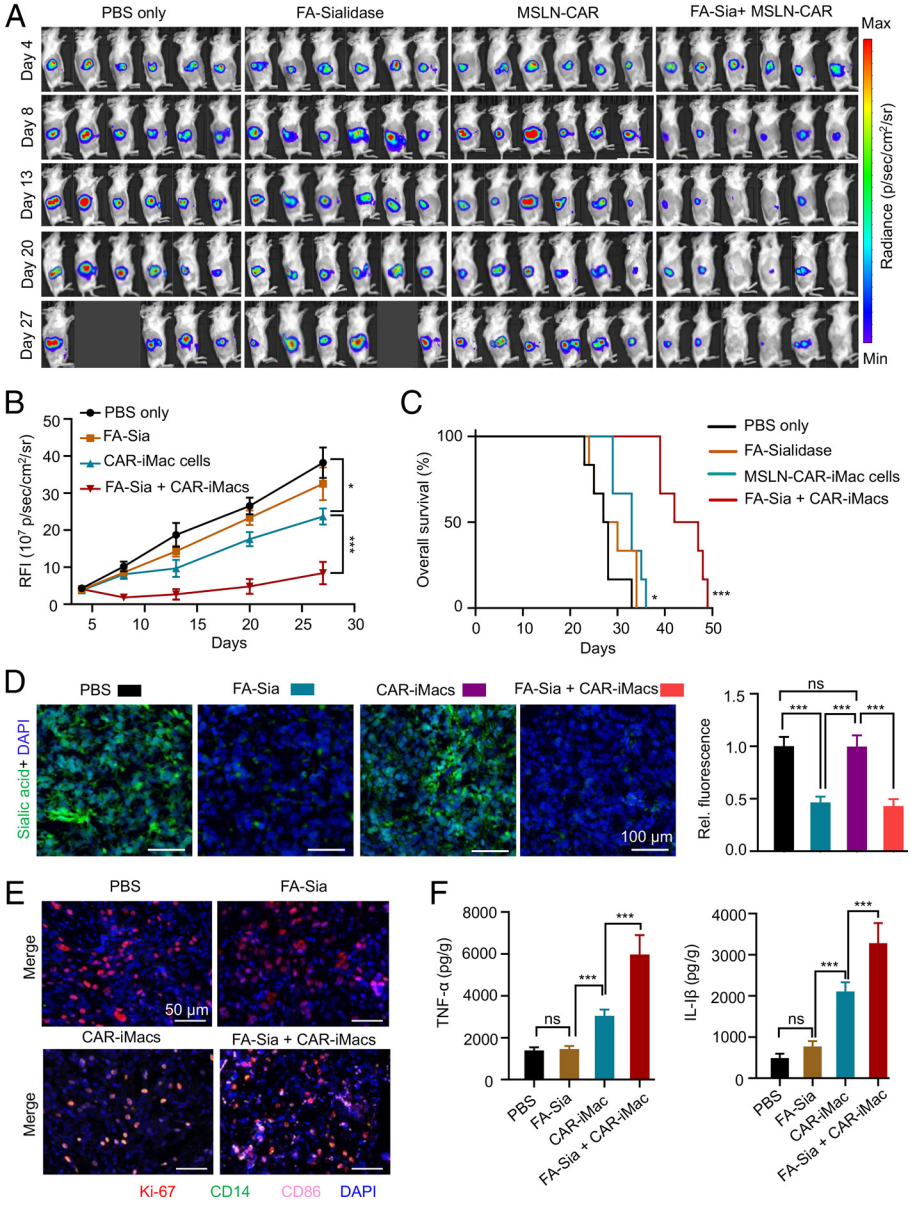

Fig. 4. The efficacy of cancer cell deglycosylation combined with CAR-iMac cellular immunotherapy in solid tumors. (*A*) Bioluminescence images of mice subjected to different treatments. (*B*) Relative fluorescence signal measured by bioluminescence imaging for different groups. (*C*) Survival of mice after CAR-iMac cellular therapy illustrated by Kaplan–Meier curves. (*D*) Detection of the sialic acid content on the surface of tumor cells. (*E*) Quantitative analysis of CD14 and CD86 fluorescence signals in the TME after different treatments. (*F*) The secretion levels of TNF-α and IL-1β in different treatment groups for orthotopic SKOV3 tumors on day 12. All data are expressed as the mean ± SD and were analyzed by one-way ANOVA with multiple comparisons correction (**P* < 0.05, ***P* < 0.01, ****P* < 0.001).

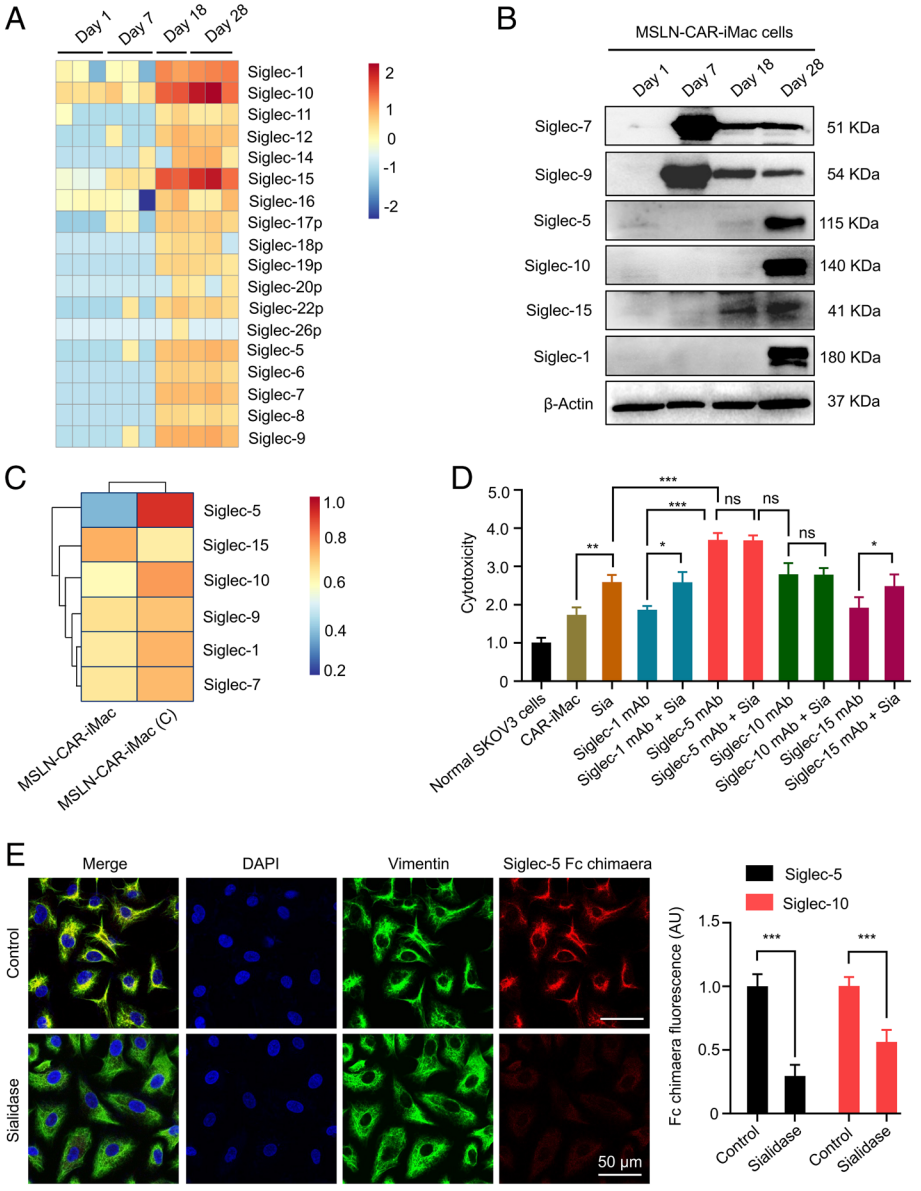

Fig. 5. Deglycosylation of cancer cells promotes phagocytosis and antitumor effects mainly via Siglec-5 and Siglec-10 recognition. (*A*) The mRNA expression levels of *Siglecs* in mesothelin-CAR-iMacs on differentiation days measured by RNA-seq. (*B*) The protein expression levels of Siglecs in CAR-iMacs on different differentiation days. (*C*) The mRNA expression levels of *Siglecs* in mature CAR-iMacs before and after exposure to cancer cells. (*D*) Cytotoxicity of CAR-iMacs to SKOV3 cells in the absence or presence of free sialidase or an anti-Siglec monoclonal antibody (Siglec-1, Siglec-5, Siglec-10, Siglec-15 mAb) at an E/T ratio of 5:1. (*E*) Detection of recombinant Siglec-5 or Siglec-10 protein binding to SKOV3 cells with or without deglycosylation. All data are expressed as the mean ± SD and were analyzed by one-way ANOVA with multiple comparisons correction (*$P < 0.05$, **$P < 0.01$, ***$P < 0.001$).

sialic acid analogs as donor substrates to generate high-affinity Siglec-5 or Siglec-10 ligands in vitro. The desialylation group was treated with sialidase, and the affinity was assessed by detecting rhodamine (TRITC)-AffiniPure IgG fluorescence. Consistent with earlier results, the results demonstrated that the sialic acid analog Neu5Acα (2–3) Gal caused significantly higher binding to Siglec-5-Fc or Siglec-10-Fc, while this binding effect could be reversed with highly active sialidase (*SI Appendix*, Fig. S14*B*). All these results suggested that cancer cell deglycosylation enhanced the antitumor effects of CAR-iMacs mainly by abolishing the collective interactions of sialylated glycans with the inhibitory receptors Siglec-5 and Siglec-10.

Glycocalyx Inhibits the Antitumor Effects of CAR-iMac Cells via Glycoimmune Checkpoint Siglec-5 and Siglec-10 Recognition. To further clarify that Siglec-5 and Siglec-10 recognition was the main contributor to the immunosuppressive phenotype, we utilized the CRISPR–Cas9 method to knock out Siglec-5 and Siglec-10 simultaneously in iPSC-derived CAR-iMac cells (Fig. 6*A*). The western blotting results demonstrated that the CAR-iMacs 28 days after differentiation did not express Siglec-5 and Siglec-10 proteins on the cell membrane after gene editing (Fig. 6*B*). Interestingly, the knockout of Siglec-5 and Siglec-10 in CAR-iMac cells (DKO-CAR) prominently reduced the percentage of macrophages polarized toward the M2-like state in vitro (Fig. 6*C*), which may be related to the release of self-contact inhibition of sialic acid on the surface of the macrophage membrane. In addition, the DKO CAR-iMacs demonstrated stronger phagocytosis activity (Fig. 6*D*) and tumor cytotoxicity (Fig. 6*E*) against ovarian cancer cells and recapitulated the increased effect of macrophage-induced ADCP upon cancer cell deglycosylation by sialidase. In addition, we used an orthotopic mouse model of ovarian tumors to assess the therapeutic potential of targeted deglycosylation of cancer cells in conjunction with the adoptive transfer of the edited CAR-iMacs in vivo. The results indicated that the DKO-CAR-iMac cells exhibited surprisingly stronger antitumor efficacy against ovarian cancer when used alone (Fig. 6 *F* and *G*), comparable to that of cancer cell deglycosylation combined with the wild-type CAR-iMac group. As expected, cancer cell deglycosylation combined with adoptive transfer of DKO-CAR-iMacs did not display further enhanced efficacy in inhibiting ovarian cancer growth (Fig. 6 *F* and *G*). Similarly, DKO-CAR-iMac adoptive cell therapy significantly prolonged mouse survival, similar to FA-Sia-induced desialylation combined with wild-type CAR-iMac

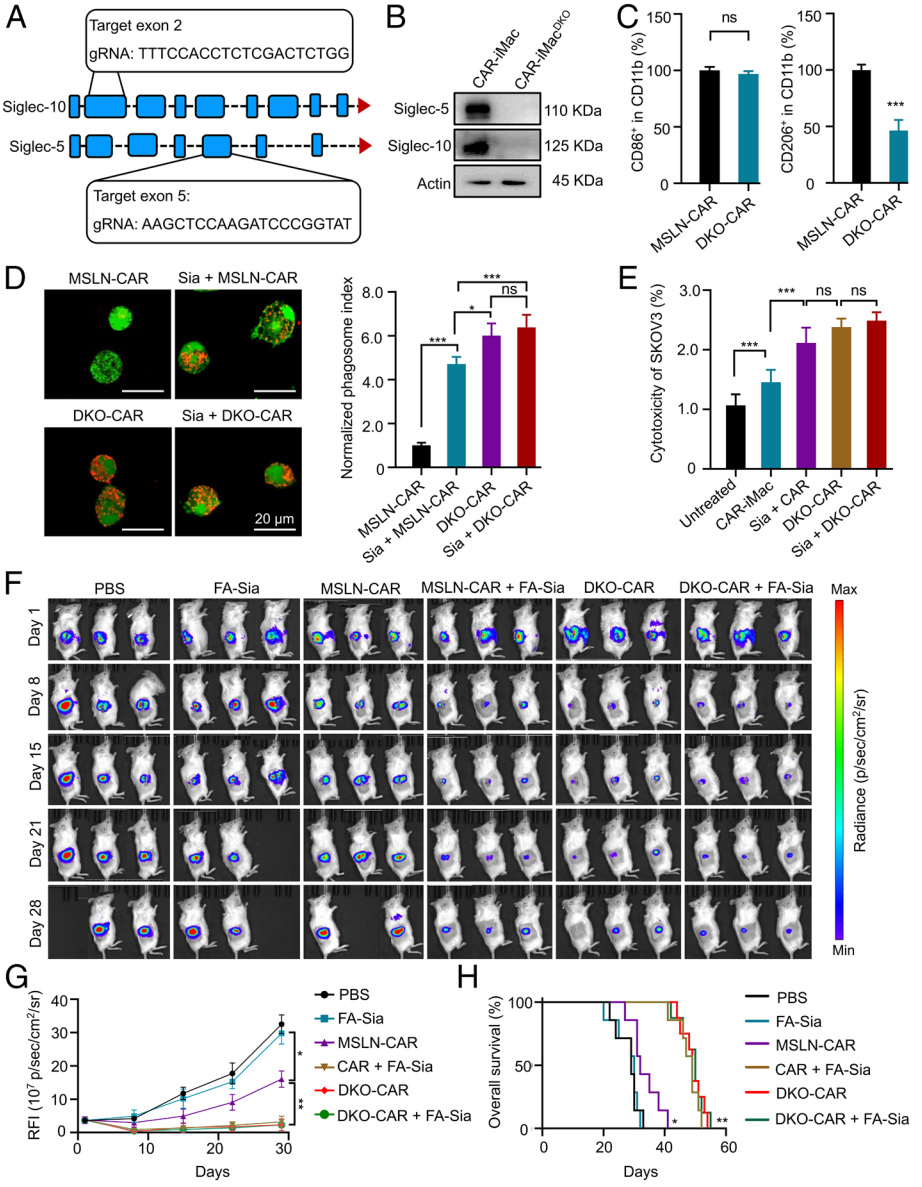

Fig. 6. Glycocalyx inhibits the antitumor effects of CAR-iMac cells via glycoimmune checkpoint Siglec-5 and Siglec-10 recognition. (*A*) The construction strategy of CRISPR–Cas9 guide RNAs for Siglec-5 and Siglec-10. (*B*) The protein expression of Siglec-5 and Siglec-10 in CAR-iMac cells on day 28 of differentiation from iPSCs with or without CRISPR-Cas9-mediated knockout of the genes. (*C*) The polarization state of CAR-iMacs after 28 d of differentiation with and without Siglec-5 and Siglec-10 knockout. (*D*) Phagosomes of CAR-iMacs coincubated with SKOV3 cells after different treatments. (*E*) Cytotoxicity of CAR-iMacs against SKOV3 cells in the absence or presence of free sialidase at an E/T ratio of 5:1. (*F*) Bioluminescence images of mice subjected to different treatments. (*G*) Relative fluorescence signal measured by bioluminescence imaging for different groups. (*H*) The survival rate of mice after CAR-iMac cellular therapy illustrated by Kaplan–Meier curves. All data are expressed as the mean ± SD and were analyzed by one-way ANOVA with multiple comparisons correction (*$P < 0.05$, **$P < 0.01$, ***$P < 0.001$).

adoptive cell therapy (Fig. 6*H*). In addition, more tumor necrosis–related cytokines were consistently detected in the DKO-CAR-iMacs and the combined treatment group (*SI Appendix*, Fig. S15). Collectively, these results suggested that cancer cell deglycosylation enhanced the antitumor effects of iPSC-derived CAR-iMac cells mainly by hindering the interactions of sialylated glycans with the inhibitory receptors Siglec-5 and Siglec-10 and that glycoimmune checkpoint receptor knockout is an effective strategy for making CAR-macrophages with stronger antitumor activity.

Deglycosylation of Cancer Cells Promotes Macrophage-Mediated Antitumor Effects in Immune-Competent Mice. To further determine the effect of desialylation on macrophage adoptive therapy in the immune competent system, we constructed a syngeneic tumor model in C57BL/6 mice with normal immune systems and achieved effective treatment by targeted deglycosylation of cancer cells combined with intravenous injection of bone marrow-derived macrophage (BMDM) cells. Before intravenous injection, C57BL/6 mouse–derived BMDMs were induced to differentiate into the M1-like state (Fig. 7*A*), and LLC-luci cells were deglycosylated with targeted sialidase. We first verified the killing ability of BMDMs on LLC cells in vitro to confirm that the culture and induction were successful (Fig. 7*B*); surprisingly, we found that desialylation significantly enhanced the cytotoxicity of activated BMDMs against LLC cells (Fig. 7*B*). Consistent with this, the in vivo results demonstrated that, compared to the control group that received buffer injection only, the group treated with targeted sialidase showed only a slight inhibition of LLC-Luci tumor growth (Fig. 7 *C* and *D*). It is interesting that BMDM adoptive cell therapy demonstrated no tumor inhibitory effect, which may be related to the induction of the M2-like polarization of BMDMs by TAMs in the inhibitory tumor microenvironment (17). However, deglycosylation of cancer cells combined with the adoptive transfer of BMDMs reversed those effects and displayed surprising efficacy in inhibiting tumor growth (Fig. 7 *D* and *E*). The number of metastatic nodules in the mice was also significantly reduced, and the survival time of tumor-bearing mice was significantly prolonged in the combined treatment group (Fig. 7*F* and *SI Appendix*, Fig. S16*A*). In accordance with these results, the modification of sialidase with targeting peptides could increase the selectivity of complex molecules to cancer cells and remove the overexpressed sialic acid from tumor nodules efficiently in a targeted fashion (*SI Appendix*, Fig. S16*B*). In addition, cancer cell desialylation selectivity combined with BMDM injection therapy promoted more M1-state macrophage

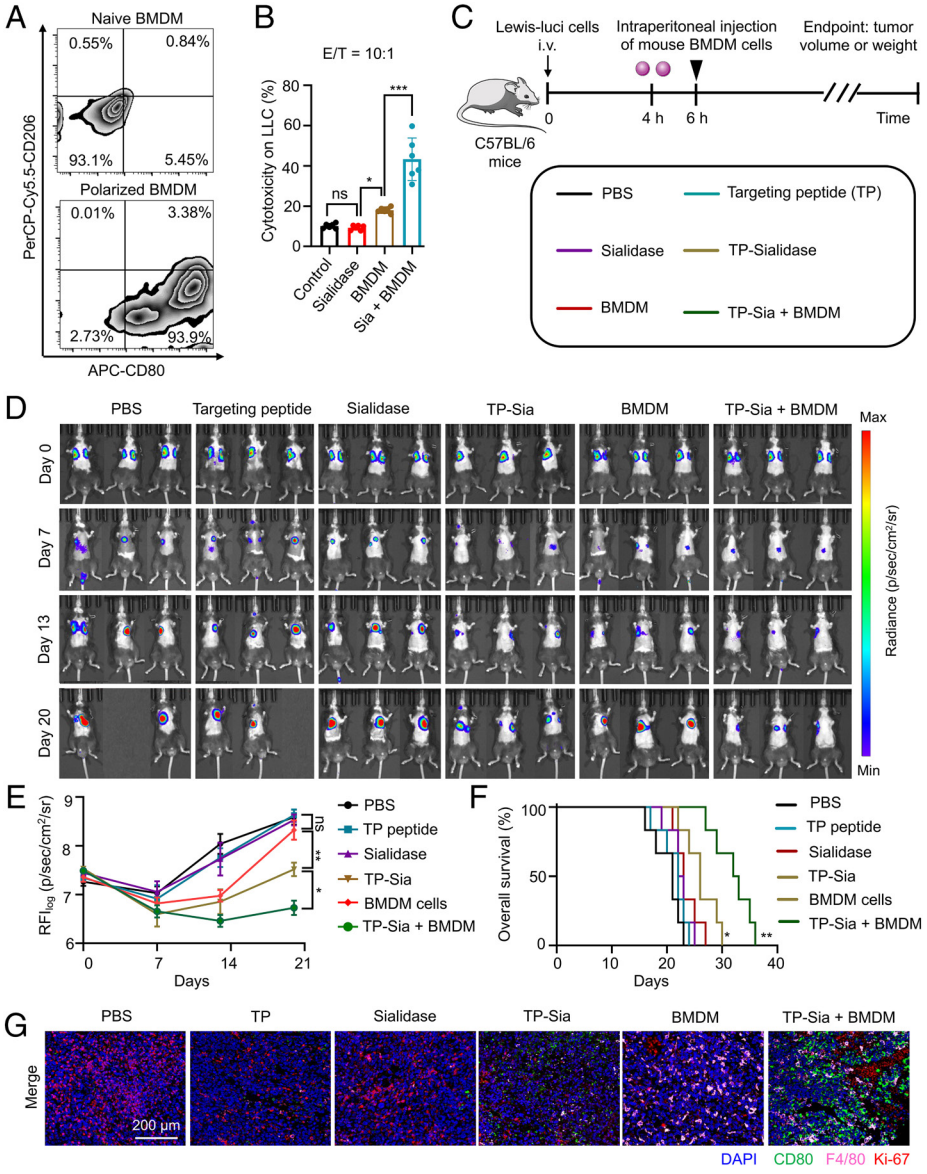

Fig. 7. Deglycosylation of cancer cells promotes macrophage-mediated antitumor effects in immune-competent mice. (*A*) Flow cytometric analysis of M2-like macrophages ($CD206^+$) and M1-like macrophages ($CD80^+$) in BMDMs gating on $F4/80^+CD11b^+CD45^+$ cells. (*B*) The cytotoxicity of activated BMDMs to LLC-Luci cells in the absence or presence of free sialidase at an E/T ratio of 10:1. (*C*) The timeline for lung metastasis tumors and cellular immunotherapy administered by intravenous injection. (*D*) Bioluminescence images of mice subjected to the different treatments. (*E*) Relative fluorescence signal measured by bioluminescence imaging for different groups. (*F*) Survival corresponds to the tumor size of mice after different treatments as indicated. (*G*) The infiltration and proliferation of immune cells in lung tumors were evaluated by staining with fluorophore-conjugated antibodies against Ki-67, CD80, and F4/80 in the absence or presence of the recombinant TP-Sia protein combined with BMDM cellular immunotherapy. All data are expressed as the mean ± SD and were analyzed by one-way ANOVA with multiple comparisons correction (*P < 0.05, **P < 0.01, ***P < 0.001).

infiltration in the cancer nest (Fig. 7*G* and *SI Appendix*, Fig. S16*C*) and induced macrophages to secrete more tumor-killing cytokines (*SI Appendix*, Fig. S16*D*). These results reconfirmed collectively that cancer cell deglycosylation could reshape the inhibitory immune microenvironment of solid tumors and enhance macrophage-mediated adoptive cell immunotherapy.

Discussion

Immune cell–based therapies have emerged as a promising approach to better treat and potentially cure malignancies that are refractory to other modalities, such as chemotherapy, surgery, or radiation therapy (18–20). Recent clinical trials include the use of engineered T lymphocytes or NK cells for the treatment of hematopoietic and solid tumors (21, 22). However, even though T cells engineered to express a CAR have demonstrated impressive potency against CD19-expressing hematological tumors, the efficacy of CAR-T cells against solid tumors remains limited (23). Macrophages are central effectors and regulators of the innate immune system and are capable of phagocytosis, cellular cytotoxicity, proinflammatory factor secretion, and antigen presentation to T cells (10). Compared to CAR-T cells, CAR-engineered NK cells or macrophages could offer several significant advantages; these potential advantages include better safety, such as no or minimal cytokine release syndrome and neurotoxicity in the autologous setting and no or minimal graft-versus-host disease in an allogenic setting, and multiple mechanisms for activating cytotoxic activity, which is regarded as a hope for cellular immunotherapy platforms against cancer (24–26).

However, macrophage-mediated cancer cell cytotoxicity is frequently regulated by a repertoire of activating and inhibitory receptors. Monoclonal antibodies that antagonize the interactions of don't eat me signals have demonstrated therapeutic potential in several cancers, but the variability in the magnitude and durability of the responses to these agents have suggested the presence of additional currently unknown don't eat me signals (27). Tumor cells can adaptively express a variety of inhibitory receptors to inhibit the activity of macrophages (don't eat me signals), and these signals include CD47, PD-L1, CD24, and CD169, which engage their cognate receptors signal regulatory protein α (SIRPα), programmed death 1 (PD-1), Siglec-1 and Siglec-10, respectively, to exert an inhibitory effect on phagocytosis (28–31). While most immune checkpoint inhibitors target protein checkpoints, cell-surface glycosylation has recently garnered interest as a mediator of immune inhibition (32, 33). Subsequent work has demonstrated that sialoglycans suppress immune activation and act as glycoimmune checkpoints through

multiple mechanisms: preventing complement-dependent cytotoxicity; inhibiting immune-mediated apoptosis through the death receptor Fas; masking immune-activating ligands of natural killer cell receptor natural killer group 2, member D (NKG2D); preventing calreticulin binding and subsequent macrophage clearance; and directly binding Siglec receptors (34–36). Functional CD169 (Siglec-1) on macrophages is a lectin receptor that binds sialylated glycoproteins and glycolipids on both endogenous cells and pathogens and mediates interactions with dendritic cells for $CD8^+$ T cell cross-priming (31, 37). Siglec-5 expressed on macrophages can participate in the phagocytosis of apoptotic bodies and is significantly inhibited by sialylated carbohydrates (38). Siglec-15 expressed on macrophages can bind with its sialic acid ligand sialyl-Tn on tumor cells, resulting in the production of TGFβ, which further magnifies the immunosuppressive effect (39). These observations highlight the implications of the Siglec-sialoglycan axis for immune modulation, and glycan degradation is emerging as an attractive target for cancer immunotherapy (33, 40).

The correlation of hypersialylation with cancer immune escape has been known for a while (34–36). Several teams have explored various sialic acid–removing enzymes for cancer therapy, but none have achieved ideal progress (41–43). This lack of progress may have several causes. First, sialidase has no cancer-targeting feature, and nonselective removal of sialic acid results in severe side effects as well as insignificant antitumor effects. Second, removal of sialic acid from the cancer cell surface often has only transitory immune-activating effects against cancer cells due to the rapid recovery of cell-surface sialic acid. Bertozzi et al. developed a series of highly active sialidases and constructed a trastuzumab-sialidase conjugate (T-Sia 2) through a hydrazino-iso-Pictet-Spengler reaction with aldehyde-tagged antibodies and copper-free click chemistry for effective sialic acid clearance and cancer therapy (33). This click-chemical modification indicated a new direction for the targeted modification of sialidase since the enzymatic activity must be maintained. A recent study by Läubli et al. demonstrated that targeted removal of Siglec ligands in the TME using the same antibody–sialidase conjugate, T-Sia 2, enhanced antitumor immunity and halted tumor progression in several murine models through repolarization of tumor-associated macrophages (44). However, studies on sialic acid–targeted clearance combined with adoptive cellular immunotherapy have rarely been reported.

In this study, we quantified the expression of sialic acid on the surface of cancer cells and designed a variety of tumor-targeted sialidase conjugates that potently and selectively stripped different sialoglycans from a variety of cancer cells. The deglycosylation of cancer cells potentiated macrophage-mediated ADCP and enhanced CAR-iMac activation and polarization, resulting in the production and release of inflammatory mediators, including TNF-α, IL-1β, and IFN-γ, in vitro. Furthermore, desialylation of cancer cells significantly enhanced the CAR-iMac- or BMDMs-mediated antitumor effect through increased infiltration of M1 macrophages and repolarization of tumor-associated macrophages. Mechanistically, as iPSC-induced macrophages matured gradually, more Siglec signals were expressed on the cell membrane, with Siglec-5 and Siglec-10 playing a crucial inhibitory role. The expression levels of Siglecs rose again after CAR-iMacs were exposed to cancer cells, which might be closely related to the abnormally high glycosylation levels of cancer cells. Targeted glycan degradation or ligand blockade also disrupted Siglec-5- and Siglec-10-mediated inhibitory signaling, changing cancer cells from an immune escape state ("cold tumor") to a sensitive recognition state ("hot tumor"). This change significantly achieved an ideal therapeutic outcome for adoptive cellular immunotherapy in solid tumors, which provides an opportunity for expanding the indications for cellular immunotherapy against solid tumors. In addition, the Siglec-5 and Siglec-10 knockout strategies not only interrupt the link between sialic acid and the inhibitory ligands but also construct a CAR-iMac cell with better cancer cell toxicity, which may bring strategies and insight for the construction of CAR macrophages and the cellular immunotherapy of solid tumors.

There is significant future potential for combining sialidase-targeting molecules that target glycoimmune checkpoints with adoptive cellular immunotherapy. The strategy of encoding and expressing an efficient sialidase on the immune cell surface to achieve targeted removal of sialic acid from cancer cells is a good method; however, avoiding sialidase removing sialic acid from the immune cell membrane itself is a difficult problem since sialic acid on the surface of immune cell membranes also plays important biological functions. Designing sialidase for sialic acid contact activation may be a good solution; however, more studies are still needed to further verify the effects of these strategies. Until that is achieved, the strategy of separate injections of the targeted sialidase molecule and cellular immunotherapy still has irreplaceable significance for cellular immunotherapy against solid tumors.

In conclusion, we developed a variety of tumor-targeted sialidase conjugates to deglycosylate cancer cells, which potentiated macrophage-mediated ADCP and enhanced CAR-iMac activation and polarization. Targeted glycan degradation or ligand blockade can disrupt Siglec-5- and Siglec-10-mediated inhibitory signaling, changing cancer cells from an immune escape state ("cold tumor") to a sensitive recognition state ("hot tumor"), which expands the indications for cellular immunotherapy against solid tumors, and Siglec-5- and Siglec-10 dual knockout strategies were utilized to construct a CAR-iMac cell with enhanced cancer cell toxicity; these results provide a perspective for effective cancer therapy in the future.

Materials and Methods

Expression and Purification of Sialidase. A protein expression plasmid was constructed according to the neuraminidase gene sequence in the NCBI database, and an *E. coli* cell–free protein system was used to express the sialidase protein (entrusted to Hangzhou Jinao Biotechnology Co., Ltd.), and the target protein was purified with a His-trap column. The purified protein was run four times through endotoxin-removal resin (Thermo Fisher), followed by buffer exchange using a PD-10 column. Then, the samples were dialyzed against 50 mM Tris-HCl (pH 8.0), 150 mM NaCl, 1 mM EDTA, and 10% glycerol buffer, and the purified protein was verified by HPLC to ensure that the protein purity was >95%.

Detecting Desialylation of Cancer Cells with SNA. Cells were rinsed with 1× DPBS buffer (Gibco), trypsinized for 5 min at 37 °C, and pelleted by centrifugation at 500 × g for 5 min. Then, the cells were washed three times with DPBS and resuspended to 1×10^6 cells per ml in serum-free DMEM. Next, 200 μL of cells was added to V-bottom 96-well plates (100 μL per cell line for mixed cell assays). Individual wells were treated with different concentrations of sialidase or an equal volume of PBS. The cells were incubated with sialidase for 1 h at 37 °C and 5% CO_2. Thereafter, the cells were harvested by centrifugation at 500 × g for 5 min and washed three times with DPBS before staining. For SNA staining, cells were resuspended in FITC-labeled *Sambucus nigra* lectin in blocking buffer (PBS and 0.5% bovine serum albumin) and incubated at 4 °C for 30 min. Then, the cells were washed three times with blocking buffer and analyzed by flow cytometry on a CytoFLEX LX flow cytometer (Beckman). Flow cytometry data were analyzed and gated to differentiate and quantify SNA^+ and SNA^- cells using FlowJo v.10.0 software (TreeStar).

Labeling and Detection of Free Sialic Acid. The fluorescent labeling and detection of free sialic acid were performed according to the LudgerTag™ DMB kit recommendations (LT-KDMB-A1). Briefly, 1×10^6 cells were treated with sufficient sialidase to obtain a suspension containing sialic acid, and then the sialidase was removed by ultrafiltration and centrifugation to obtain free sialic acid. Next, 5 μL of free sialic acid was obtained by the above reaction, and 20 μL of DMB

molecules was added. Then, the mixture was reacted in the dark for 3 h under acidic conditions at a constant temperature. Then, a certain amount of distilled water was added to terminate the reaction. The reaction products were run on a LudgerSep™ R1 HPLC column (λ ex = 373 nm, λ em = 448 nm). A 30-min isocratic elution with temperature control at 30 °C was recommended, and the flow rate was recommended to be 0.5 mL/min. In addition, the recommended separation solvent was methanol:acetonitrile:water (7:9:84 v/v). The standard sialic acid product in the kit was used to generate standard curves for concentration and peak area, and the content of the sialic acid product on the surface of different cancer cells was calculated according to the peak of the standard product.

Synthesis of the TP-Sia Complex Molecule. Fifty milligrams of sialidase (90 kDa) was weighed and dissolved in PBS-EDTA solution, and the free carboxyl group was calculated according to the amino acid sequence. Then, a specific weight of Sulfo-LC-SPDP (Thermo Scientific) powder was weighed and added to the solution according to the molar ratio of the carboxyl group at 1:10. After the solution was stirred in the dark and reacted at 16 °C overnight, Millipore Merck Amicon® Ultra15 10-kDa ultrafiltration centrifuge tubes were used for segregation at 3,500 × g for 20 min to remove any unreacted Sulfo-LC-SPDP Linker. Next, an accurate quantity of non-small cell lung cancer-TP (CTDSILRSYDWTY) was weighed and added to the solution at a molar ratio of 1:10, and the mixture was magnetically stirred at 16 °C for 24 h to allow coupling. Then, the mixture was centrifuged with an ultrafiltration tube to remove any unconnected TP. Finally, the obtained targeting complex molecules were lyophilized, and NMR and infrared spectroscopy (IR) were employed to determine whether the complex molecules (TP-Sia) were successfully synthesized. Before the complex molecules (TP-Sia) were used, FITC-modified SNA was also employed to detect the enzymatic activity.

Synthesis of the FA-Sia Complex Molecule. A total of 50 mg of sialidase was weighed and dissolved in PBS-EDTA solution, and the free carboxyl group was calculated according to the amino acid sequence. Then, the reagents 1-(3-dimethylaminopropyl)-3-ethylcarbodiimide hydrochloride (EDC) and sulfo-1-hydroxy-2,5-dioxopyrrolidine-3-sulfonic acid (Sulfo-NHS) were added to the solution according to the molar ratio of the carboxyl group at 1:10. The mixture was magnetically stirred at 16 °C for 24 h to activate the carboxyl group, and then folic acid was added to the solution according to the molar ratio of the carboxyl group at 1:10. The mixture was magnetically stirred at 16 °C for 24 h again to allow coupling. Any unconnected folic acid was removed by centrifugation with an ultrafiltration tube (Millipore Merck Amicon® Ultra15 10K), and the obtained target complex molecules were lyophilized. Before use, FITC-modified SNA was used to detect the enzymatic activity, and NMR was used to detect whether the complex molecule was successfully synthesized.

Fluorescence Detection of Sialic Acid in Tumors. The quantitative analysis of sialic acid content in tumors was performed according to the ref. 45. Briefly, fresh tumor tissues from the mice in different treatment groups were cut into slices with a thickness of 5 μm under a Leica CM1850 microtome. Next, 4% paraformaldehyde was added dropwise to the slices to fix for 5 min. Then, the slices were washed three times in PBS solution, and 100 μL of $NaIO_4$ working solution was added dropwise to the sliced tissue and reflected at 4 °C for 20 min. Next, 0.5 mL of glycerol working solution was added dropwise to the slices. Then, the slices were rinsed three times with cold PBS, and 20 μL of FTSC working solution was added dropwise to the tissue. The slices were placed in a 37 °C incubator for 40 min. After three washes with PBST, DAPI (1:2,000 dilution) was added immediately to the cells before they were coverslipped with an antifluorescence quencher, and images were taken under an Olympus BX51 microscope.

Flow Cytometry-Based Phagocytosis Assay. All in vitro phagocytosis assays reported here were performed by coculturing target cells and donor-derived macrophages at a ratio of 100,000 target cells to 50,000 macrophages in serum-free Iscove's modified Dulbecco's medium (IMDM, Life Technologies, USA) for 4 h in a humidified, 5% CO_2 incubator at 37 °C in ultralow-attachment 96-well U-bottom plates (Corning, USA). In brief, MSLN-CAR-iMac cells with endogenous fluorescence (green fluorescent protein) were collected from plates using TrypLE Express (Life Technologies). SKOV3 cells that lacked endogenous fluorescence were collected and labeled with PKH26 (Invitrogen, USA) by suspending the cells in PBS + 1:20,000 PKH26 per the manufacturer's instructions. Then, the cells were washed twice with 5 mL of PBS to remove the residual fluorescence. Before coculture, the deglycosylation group of SKOV3 cells was pretreated with high-potency sialidase for 30 min, while the control group was pretreated with DMEM without serum. Flow cytometry and confocal microscopy were used to analyze the phagocytosis capacity or phagosome formation of CAR-iMac macrophages.

In Vitro Binding Assay for Sialic Acid Molecules and Siglec-5-Fc Chimeras. Sulfhydryl-containing sialic acid complexes [Neu5Acα(2–3)Gal-β-HHHHHC, 0.5 mg/mL; Guoping Pharmaceutical Co., China] were incubated with 0.1 mg/mL gold nanoparticles (XFNANO Materials Tech. Co., Ltd., XFJ60-11) in vitro at 37 °C for 24 h. Then, the complexes were centrifuged at 3,000 × g for 15 min to remove any unbound sialic acid complexes and gently washed with PBS three times. Then, an appropriate concentration of Siglec-5-Fc chimeras or 10-Fc chimeric protein preincubated with TRITC-AffiniPure goat anti-human IgG was added to bind the sialic acid complexes, and sialidase was added to the control group at the same time. Finally, the resuspended complexes were plated in a black 96-well plate, and the Siglec recombinant protein content adsorbed on the surface of the gold nanoparticles was detected by an M5 microplate reader at 573 nm.

Luciferase-Based Cytotoxicity Assay. A total of 5×10^4 SKOV3-luci cells were mixed with cultures of engineered CAR-iMacs, polarized CAR-iMacs (pretreatment with 50 ng/mL TNF-α for 4 h and 100 ng/mL LPS for 24 h before use) or NK-92 cells (pretreatment with 100 ng/mL recombinant human IL-2 for 24 h before using) at an effector/target (E/T) ratio of 10:1. The mixtures were then cultured in round-bottom 96-well plates for 24 h, centrifuged to remove the supernatant (which was collected for quantification of cytokine production), and assayed with a bright-glo luciferase assay system (Promega, E2610) following the manufacturer's instructions to quantify the luminescence of each sample. The cytotoxicity (%) of sample X was calculated as (1- luminescence of X/luminescence of "target cell only") × 100%.

Generation of CRISPR-Cas9 knockout iPSCs. CRISPR—Cas9 guide RNAs were designed for Siglec-5 and Siglec-10 genome sequences, and the LentiCRISPRv2 KO plasmid was constructed for Siglec-5 and Siglec-10 deletion. For transfection, the single sgRNA vectors, envelope vector pMD2. G, and packaging vector psPAX2 were mixed in a 4:3:1 ratio in OPTI-MEM (Thermo Fisher Scientific, 31985070) and PEI (Polysciences, 9002-98-6) and transfected into HEK293T cells at 80 to 90% confluence in 10-cm tissue culture plates. The supernatant was collected at 24, 48, and 72 h posttransfection, filtered via a 0.45-μm filtration unit (Millipore, Cat# SLHVR33RB), and mixed overnight at 4 °C with one-third volume of 30% PEG8000. The medium was concentrated at 4,200 rpm for 30 min at 4 °C. The pellet was resuspended in PBS and stored at −80 °C. Then, iPSCs were infected with lentivirus expressing Cas9 and sgRNAs targeting Siglec-5 and Siglec-10 and 5 μg/mL polybrene overnight, and the medium was changed the following day. After puromycin (250 ng/mL) selection for three days, the iPSCs were digested into single cells and seeded into six-well plates (2,000 cells/well). Five days later, single clones were picked and transferred to 96-well plates and then verified by Sanger sequencing and western blotting.

Isolation and Activation of Primary BMDM cells. Mouse primary BMDMs were isolated from C57BL/6 mouse bone marrow. Following isolation, primary BMDMs were cultured in RPMI-1640 supplemented with 10% heat-inactivated FBS and 25 ng/mL mouse MC-GSF (PeproTech) for 7 d. Before use, 100 ng/mL LPS (MedChemExpress) and 50 ng/mL IFN-γ (PeproTech) were used to treat BMDMs for 24 h to induce BMDMs to the M1 type. Typical markers, including CD11b, F4/80, CD80, and CCR2, were considerably detected in M1-BMDMs. After activation, the M1-BMDM cells were cocultured with LLC-luci cells in kill tests or injected intravenously to treat in situ lung cancer in mice.

Xenogenic Mouse Models. We used a NOD-Prkdc scid IL2rg tm1/Bcgen (NSG; Shanghai Model Organisms Center, Inc.) mouse model to assess the in vivo antitumor effect of transduced CAR-iMacs. All animal experiments were conducted according to a protocol approved by the Zhejiang University Animal Care and Use Committee (Approval Number: 2020-137), and all experiments complied with relevant ethical regulations. To investigate the antitumor activity of CAR-iMacs in vivo, 6- to 8-wk-old female NSG mice were intraperitoneally inoculated (s.c.) in the right lower quadrant with 5×10^5 SKOV3-luci cells in 100 μL of 50:50 Matrigel (Corning) and PBS. Desialylated SKOV3 cells were pretreated with sialidase for 1 h prior to injection. Four hours after cancer cell inoculation, 5×10^6 MSLN-CAR-iMacs pretreated with 50 ng/mL INF-γ and LPS for 4 h were inoculated intraperitoneally to assess CAR-iMac-based killing. Then, the mice were imaged on day 1, day 7, day 14, and day 21 after cancer cell inoculation for

45 s using an IVIS system (IVIS, Xenogen Corp, Alameda, CA) under isoflurane anesthesia, and 1.0 μmol 8pyDTZ (MCE, Co., Ltd.) in 100 μL of normal saline was intraperitoneally injected.

Orthotopic Ovarian Cancer Model. Six- to eight-week-old female NSG mice were employed to assess the in vivo antitumor effect of transduced CAR-iMacs. Briefly, the right abdominal cavity of NSG mice was opened under continuous inhaled isoflurane anesthesia, and then the right ovary was gently exposed. A microinjector (Gairdner, 3-00250) was used to slowly inject 2.5×10^5 SKOV3-luci cells in 20 μL of 10:10 Matrigel (Corning) and PBS. On day 4, the mice were intraperitoneally (i.p.) infused with 1.0 μmol 8pyDTZ (MCE, Co., Ltd.) in 100 μL of normal saline, anesthetized with isoflurane and imaged with an in vivo imaging system (IVIS) with Living Image software (PerkinElmer). Then, 5×10^6 transduced CAR-iMacs (in 200 μL of PBS) were adoptively transferred into tumor-bearing mice via the tail vein. For the combined administration experiment, 0.2 μM (in 100 μL of PBS) FA-Sia conjugated proteins were adoptively transferred into tumor-bearing mice via the tail vein to ensure a desialylated condition before CAR-iMacs were injected 2 h later. To strengthen the therapeutic effect, the same amount of CAR-iMacs was injected again after 5 d, and the mice were reanalyzed with the IVIS once a week.

Statistical Analyses. The results are expressed as the mean ± SD. Statistical analysis was performed using SPSS 18.0 for Windows (SPSS Inc., Chicago, IL, USA). Comparisons among different groups were performed by one-way ANOVA with multiple comparisons correction. The survival of mice with carcinomas was compared using the Kaplan–Meier method, and differences between survival curves were tested using the log-rank test. Differences between experimental and control groups were considered statistically significant at $P < 0.05$. Statistical significance is indicated as follows: $^*P < 0.05$, $^{**}P < 0.01$, and $^{***}P < 0.001$.

Data, Materials, and Software Availability. All study data are included in the article and/or *SI Appendix*.

ACKNOWLEDGMENTS. We are grateful to the staff of the Core Facilities of the Institute of Translational Medicine of Zhejiang University for assisting with flow cytometry, confocal laser scanning microscopy, microplate spectrophotometry, and fluorescence microscopy. This study was supported by the National Key R&D Program of China (2022YFC3401600 and 2022YFE0121600), the Leading Innovative and Entrepreneur Team Introduction Program of Zhejiang (2022R01002), the Natural Science Foundation of China (22277107, 82188102, 82373238), the Natural Science Foundation of Zhejiang Province (LZ21H160002), and the Fundamental Research Funds for the Central Universities of China (226-2022-00168).

Author affiliations: [a]Cancer Institute (Key Laboratory of Cancer Prevention and Intervention, China National Ministry of Education), The Second Affiliated Hospital, Zhejiang University School of Medicine, Hangzhou 310009, China; [b]Institute of Translational Medicine, Zhejiang University, Hangzhou 310029, China; [c]Cancer Center, Renmin Hospital of Wuhan University, Wuhan 430060, China; [d]Center for Stem Cell and Regenerative Medicine, Department of Basic Medical Sciences, and The First Affiliated Hospital, Zhejiang University School of Medicine, Hangzhou 310058, China; [e]Liangzhu Laboratory, Zhejiang University Medical Center, Hangzhou 311121, China; [f]Ultrasonic Department, Renmin Hospital of Wuhan University, Wuhan 430060, China; [g]Quanzhou First Hospital Affiliated to Fujian Medical University, Quanzhou 362000, China; and [h]Cancer Cancer, Zhejiang University, Hangzhou 310029, China

1. R. Schauer, J. P. Kamerling, Exploration of the sialic acid world. *Adv. Carbohydr. Chem. Biochem.* **75**, 1–213 (2018).
2. U. Rutishauser, Polysialic acid at the cell surface: Biophysics in service of cell interactions and tissue plasticity. *J. Cell Biochem.* **70**, 304–312 (1998).
3. B. Byrne, G. G. Donohoe, R. O'Kennedy, Sialic acids: Carbohydrate moieties that influence the biological and physical properties of biopharmaceutical proteins and living cells. *Drug Discov. Today* **12**, 319–326 (2007).
4. M. S. Macauley, P. R. Crocker, J. C. Paulson, Siglec-mediated regulation of immune cell function in disease. *Nat. Rev. Immunol.* **14**, 653–666 (2014).
5. J. V. Pluvinage *et al.*, CD22 blockade restores homeostatic microglial phagocytosis in ageing brains. *Nature* **568**, 187–192 (2019).
6. D. Aminoff, W. F. Bruegge, W. C. Bell, K. Sarpolis, R. Williams, Role of sialic acid in survival of erythrocytes in the circulation: Interaction of neuraminidase-treated and untreated erythrocytes with spleen and liver at the cellular level. *Proc. Natl. Acad. Sci. U.S.A.* **74**, 1521–1524 (1977).
7. J. W. Dennis, S. Laferte, Tumor cell surface carbohydrate and the metastatic phenotype. *Cancer Metastasis Rev.* **5**, 185–204 (1987).
8. B. A. H. Smith, C. R. Bertozzi, The clinical impact of glycobiology: Targeting selectins, Siglecs and mammalian glycans. *Nat. Rev. Drug Discov.* **20**, 217–243 (2021).
9. L. Zhang *et al.*, Pluripotent stem cell-derived CAR-macrophage cells with antigen-dependent anti-cancer cell functions. *J. Hematol. Oncol.* **13**, 153 (2020).
10. N. R. Anderson, N. G. Minutolo, S. Gill, M. Klichinsky, Macrophage-based approaches for cancer immunotherapy. *Cancer Res.* **81**, 1201–1208 (2021).
11. W. D. Lin *et al.*, Sialylation of CD55 by ST3GAL1 facilitates immune evasion in cancer. *Cancer Immunol. Res.* **9**, 113–122 (2021).
12. W. Weidemann, J. Hering, D. Bennmann, A. Thate, R. Horstkorte, The key enzyme of the sialic acid metabolism is involved in embryoid body formation and expression of marker genes of germ layer formation. *Int. J. Mol. Sci.* **14**, 20555–20563 (2013).
13. Y. Myojin *et al.*, ST6GAL1 is a novel serum biomarker for lenvatinib-susceptible FGF19-driven hepatocellular carcinoma. *Clin. Cancer Res.* **27**, 1150–1161 (2021).
14. O. Le Saux, I. Ray-Coquard, S. I. Labidi-Galy, Challenges for immunotherapy for the treatment of platinum resistant ovarian cancer. *Semin. Cancer Biol.* **77**, 127–143 (2021).
15. A. Mantovani, P. Allavena, F. Marchesi, C. Garlanda, Macrophages as tools and targets in cancer therapy. *Nat. Rev. Drug Discov.* **21**, 799–820 (2022).
16. J. Wu *et al.*, Bioinspired tumor calcification enables early detection and elimination of lung cancer. *Adv. Fun. Mater.* **31**, 2101284 (2021).
17. C. W. T. Shields, *et al.*, Cellular backpacks for macrophage immunotherapy. *Sci. Adv.* **6**, eaaz6579 (2020).
18. R. L. Sabado, S. Balan, N. Bhardwaj, Dendritic cell-based immunotherapy. *Cell Res.* **27**, 74–95 (2017).
19. J. R. Westin *et al.*, Efficacy and safety of CD19-directed CAR-T cell therapies in patients with relapsed/refractory aggressive B-cell lymphomas: Observations from the JULIET, ZUMA-1, and TRANSCEND trials. *Am. J. Hematol.* **96**, 1295–1312 (2021).
20. K. Kingwell, CAR T therapies drive into new terrain. *Nat. Rev. Drug Discov.* **16**, 301–304 (2017).
21. R. Grosser, L. Cherkassky, N. Chintala, P. S. Adusumilli, Combination immunotherapy with CAR T cells and checkpoint blockade for the treatment of solid tumors. *Cancer Cell* **36**, 471–482 (2019).
22. K. Pan *et al.*, CAR race to cancer immunotherapy: From CAR T, CAR NK to CAR macrophage therapy. *J. Exp. Clin. Cancer Res.* **41**, 119 (2022).
23. R. G. Majzner *et al.*, CAR T Cells Targeting B7–H3, a pan-cancer antigen, demonstrate potent preclinical activity against pediatric solid tumors and brain tumors. *Clin. Cancer Res.* **25**, 2560–2574 (2019).
24. M. Daher, K. Rezvani, Outlook for new CAR-based therapies with a focus on CAR NK cells: What lies beyond CAR-engineered T cells in the race against cancer. *Cancer Discov.* **11**, 45–58 (2021).
25. Y. Gong, R. G. J. Klein Wolterink, J. Wang, G. M. J. Bos, W. T. V. Germeraad, Chimeric antigen receptor natural killer (CAR-NK) cell design and engineering for cancer therapy. *J. Hematol. Oncol.* **14** (2021).
26. M. Klichinsky *et al.*, Human chimeric antigen receptor macrophages for cancer immunotherapy. *Nat. Biotechnol.* **38**, 947–953 (2020).
27. M. Feng *et al.*, Phagocytosis checkpoints as new targets for cancer immunotherapy. *Nat. Rev. Cancer* **19**, 568–586 (2019).
28. M. E. W. Logtenberg, F. A. Scheeren, T. N. Schumacher, The CD47-SIRPalpha immune checkpoint. *Immunity* **52**, 742–752 (2020).
29. S. R. Gordon *et al.*, PD-1 expression by tumour-associated macrophages inhibits phagocytosis and tumour immunity. *Nature* **545**, 495–499 (2017).
30. A. A. Barkal *et al.*, CD24 signalling through macrophage Siglec-10 is a target for cancer immunotherapy. *Nature* **572**, 392–396 (2019).
31. D. van Dinther *et al.*, Functional CD169 On macrophages mediates interaction with dendritic cells for CD8(+) T cell cross-priming. *Cell Rep.* **22**, 1484–1495 (2018).
32. P. R. C. Imbert *et al.*, An acquired and endogenous glycocalyx forms a bidirectional "don't eat" and "don't eat me" barrier to phagocytosis. *Curr. Biol.* **31**, 77–89.e5 (2021).
33. M. A. Gray *et al.*, Targeted glycan degradation potentiates the anticancer immune response in vivo. *Nat. Chem. Biol.* **16**, 1376–1384 (2020).
34. A. Varki, P. Gagneux, Multifarious roles of sialic acids in immunity. *Ann. N. Y. Acad. Sci.* **1253**, 16–36 (2012).
35. O. M. Pearce, H. Laubli, Sialic acids in cancer biology and immunity. *Glycobiology* **26**, 111–128 (2016).
36. E. Rodriguez *et al.*, Sialic acids in pancreatic cancer cells drive tumour-associated macrophage differentiation via the Siglec receptors Siglec-7 and Siglec-9. *Nat. Commun.* **12**, 1270 (2021).
37. L. J. Edgar, N. Kawasaki, C. M. Nycholat, J. C. Paulson, Targeted delivery of antigen to activated CD169(+) macrophages induces bias for expansion of CD8(+) T cells. *Cell Chem. Biol.* **26**, 131–136 e134 (2019).
38. S. R. Ali *et al.*, Siglec-5 and Siglec-14 are polymorphic paired receptors that modulate neutrophil and amnion signaling responses to group B Streptococcus. *J. Exp. Med.* **211**, 1231–1242 (2014).
39. J. Sun, Q. Lu, M. F. Sanmamed, J. Wang, Siglec-15 as an emerging target for next-generation cancer immunotherapy. *Clin. Cancer Res.* **27**, 680–688 (2021).
40. C. Bull *et al.*, Sialic acid blockade suppresses tumor growth by enhancing T-cell-mediated tumor immunity. *Cancer Res.* **78**, 3574–3588 (2018).
41. H. H. Sedlacek, F. R. Seiler, Immunotherapy of neoplastic diseases with neuraminidase: Contradictions, new aspects, and revised concepts. *Cancer Immunol. Immun.* **5**, 153–163 (1978).
42. F. C. Sparks, J. H. Breeding, Tumor regression and enhancement resulting from immunotherapy with Bacillus Calmette-Guérin and Neuraminidase. *Cancer Res.* **34**, 3262–3269 (1974).
43. C. D. Rillahan *et al.*, Global metabolic inhibitors of sialyl- and fucosyltransferases remodel the glycome. *Nat. Chem. Biol.* **8**, 661–668 (2012).
44. M. A. Stanczak *et al.*, Targeting cancer glycosylation repolarizes tumor-associated macrophages allowing effective immune checkpoint blockade. *Sci. Transl. Med.* **14**, eabj1270 (2022).
45. Y. Zhang, J. Yuan, J. Song, Z. Wang, L. Huang, An efficient method for selectively imaging and quantifying in situ the expression of sialylated glycoproteins on living cells. *Glycobiology* **23**, 643–653 (2013).